Anion Size Modulates the Structure of the A State of Cytochrome *c*

Roberto Santucci,*,‡ Cristiana Bongiovanni,§ Giampiero Mei,|| Tommaso Ferri,⊥ Francesca Polizio,§ and Alessandro Desideri§

Dipartimento di Medicina Sperimentale e Scienze Biochimiche; Dipartimento di Biologia e INFM; Università di Roma "Tor Vergata", V. Tor Vergata 135, 00133 Roma, Italy, and Dipartimento di Chimica, Università di Roma "La Sapienza", 00185 Rome, Italy

Received March 6, 2000; Revised Manuscript Received August 10, 2000

ABSTRACT: Several studies have shown that anions induce collapse of acid-denatured cytochrome *c* into the compact A state having the properties of the molten globule and that the anion charge is the main determinant for the A state stabilization. The results here reported show that the anion size plays a role in determining the overall structure of the A state. In particular, small anions induce formation of an A state in which the native Met80−Fe(III) axial bond is recovered and the nativelike redox properties restored. On the other hand, the A state stabilized by large anions shows a histidine (His26 or His33) as the sixth ligand of the heme-iron, a very weak interaction between Trp59 and the heme propionate, and lacks nativelike redox properties. The two anion-stabilized states show similar stability, indicating that (i) the hydrophobic core (which is equally stabilized by all the anions investigated, independently of their size) is the region that mainly contributes to the macromolecule stabilization, and (ii) the flexible loops are responsible for the spectroscopic (and, thus, structural) and redox differences observed.

The high cooperativity and complexity of the protein folding process makes the characterization of conformational transitions and intermediate states hard to achieve, partly due to the limitations of the experimental approach (*1*−*3*). Characterization of equilibrium intermediates provides a direct and useful method to better elucidate the mechanism of protein folding; in recent years, a number of equilibrium intermediates has been detected and characterized, thus permitting a correlation with the kinetic folding intermediates (*4*). Several studies on folding, focused on the structural characterization of equilibrium intermediates, suggest that molten globule, a compact state with a significant amount of ordered secondary conformation but fluctuating tertiary conformation (*2*, *4*−*6*), is a major intermediate of protein folding (*7*−*10*).

The molten globule (A state) of ferric cytochrome *c* (cyt *c*),[1] a single-chain hemoprotein composed by 104 amino acidic residues, has been extensively characterized (*11*−*15*). At pH 2.2, ferric cyt *c* is substantially unfolded at low ionic strength; upon addition of salts, the protein cooperatively folds to a compact structure, the A state, stabilized by the binding of anions to the positively charged groups on the protein surface (*11*, *12*). The A state possesses α-helix structure comparable to that of the native form, but a fluctuating tertiary conformation. In particular, the hydrophobic core containing the two major helices (the N- and C-terminal helices) and the heme group is preserved in the A state, stabilized by nonbonded interactions (*13*, *16*, *17*), while the loop regions are fluctuating and partly disordered (*13*). Of the two native axial ligands of the heme-iron, only His18 is thought to remain coordinated to the heme iron in the A state, while the Met80 axial bond is lost (*11*, *13*, *18*).

Goto and collaborators (*12*) have shown that the net charge of the anion is the main determinant for the stabilization of the A state; the higher the charge, the lower the anion concentration needed to induce formation of the molten globule. Some effect was ascribed to the anion size (folding occurs at lower concentrations of larger anions); however, this point was not furtherly investigated, the ion size having being considered a minor effector.

Since structural information on partially folded forms is essential for a deeper understanding of the folding mechanism and the factors affecting the structural stabilization, in this paper we have investigated the effect produced on acid denatured cyt *c* by a number of anions carrying the same charge but differing in size. The choice of single-charged anions excludes the charge effect, and allows determination of the role played by the ion size in affecting the structural and functional properties of the molten globule. The results obtained show that this is an important factor in determining the shape of the tertiary structure and the redox properties of the A state. Small anions induce formation of a compact, highly structured state, in which the native Met80−Fe(III) axial bond is recovered, with nativelike redox properties. On the other hand, large anions stabilize a compact, bis-histidine state, lacking the redox properties of the native protein. A correlation of these results with the sequential folding model of Englander and collaborators (*19*), is discussed.

* To whom correspondence should be addresssed. Phone: +39 06 72596364. Fax: +39 06 72596353. E-mail: santucci@med.uniroma2.it.

‡ Dipartimento di Medicina Sperimentale e Scienze Biochimiche, Università di Roma "Tor Vergata".

|| Dipartimento di Medicina Sperimentale e Scienze Biochimiche e INFM, Università di Roma "Tor Vergata".

§ Dipartimento di Biologia e INFM; Università di Roma "Tor Vergata".

⊥ Dipartimento di Chimica, Università di Roma "La Sapienza".

[1] cyt *c*, Cytochrome *c*; CD, circular dichroism; EPR, electronic paramagnetic resonance; Im-complex, imidazole-complex.

10.1021/bi000516v CCC: $19.00
Published on Web 09/21/2000

EXPERIMENTAL PROCEDURES

Materials. Horse cyt *c* (type VI) and 6-mercaptopurine (6-MP) were from SIGMA (St. Louis, MO). All the reagents were of analytical grade and used without further purification.

Circular Dichroism (CD) Measurements. Measurements were carried out using a Jasco J-710 spectropolarimeter (Tokyo, Japan) equipped with a PC as data processor. The molar ellipticity (deg cm^2 dmol^{-1}) is expressed as $[\theta]_h$ on a molar heme basis in the Soret (380−450 nm) and near-UV (270−300 nm) regions and as mean residue ellipticity $[\theta]_a$ in the far-UV region (200−250 nm, mean residue molecular mass = 119 g/mol).

Absorbance Measurements. A Jasco V-530 spectrophotometer (Tokyo, Japan) was used for absorbance measurements. Native cyt *c* concentration was determined on the basis of the extinction coefficient $\epsilon = 106$ mM^{-1} cm^{-1} at 408 nm.

Electronic Paramagnetic Resonance (EPR) Measurements. EPR spectra were recorded on a Bruker ESP 300 X-band spectrometer operating at 9 GHz with 100 Khz field modulation. An Oxford Instruments liquid helium transfer line was used for the measurements at 5 K.

Dynamic Fluorescence Measurements. The fluorescence emission decay was measured by the phase-shift and demodulation technique as elsewhere described (*20*), using as excitation source the harmonic content of a frequency-doubled rhodamine 6G-Nd:YAG laser (λ_{ex} approximately 290 nm) at the LASP (Laboratorio di Spettroscopia al Picosecondo) facility at the University of "Tor Vergata" in Rome. The emission was detected trough a WG 320 cutoff filter to avoid scattered light. A discrete sum of exponential functions

$$f(t) = \sum_{i=1}^{n} F_i e^{-t/\tau_i}$$

was necessary to satisfactorily fit the data using the GLOBAL Unlimited software (*21*), where for each component τ_i represented the lifetime value.

Voltammetric Measurements. Voltammetric measurements were performed at 25 °C in a glass microcell (sample volume 1 mL) equipped with a reference calomel electrode (Amel, Milan, Italy), a Pt wire as the counter-electrode and a gold electrode (2 mm diameter, Amel) as the working electrode.

Chemical modification of the gold electrode was obtained as previously reported (*22*). Briefly, the electrode (previously cleaned with 0.3 μm alumina plus water and sonicated) was dipped in a saturated aqueous 6-MP solution for 15 min. The electrode was then rinsed with distilled water and dipped in the electrochemical cell containing the protein solution. Before the voltammetric experiment, the solution was deaerated for 30 min by a gentle flow of pure nitrogen maintained just above the solution surface.

An Amel 433/W multipolarograph (Milan, Italy) interfaced with a PC, was employed for voltammetric measurements.

pH Measurements. A Crison 2001 pH meter (Alella, Spain) was used for pH measurements.

Samples Preparation. Samples were prepared as follows. (a) CD measurements (protein concentration: 5 μM): 4 μL of a 1 mM cyt *c* aqueous solution was added to an aqueous HCl solution, pH 2.2, and the volume brought to 2 mL (with aqueous HCl, pH 2.2) after addition of few microliters of a concentrated salt solution, to achieve the desired salt concentration (0.5 M chloride and 0.2 M perchlorate). The pH of the sample (i.e., pH 2.2) was always controlled before measurements. (b) Voltammetric measurements (protein concentration 0.4 mM: 100 μL of a 4 mM cyt *c* aqueous solution was added to 0.5 mL of an aqueous HCl solution, pH 2.2. The pH raised to above pH 3.0, while the protein solution kept a reddish color. The pH was thus brought back to pH 2.2 (the color of the solution changed to brown) and the desired salt concentration achieved by adding a few microliters of a concentrated aqueous salt solution. The volume was then brought to 1 mL and the pH controlled.

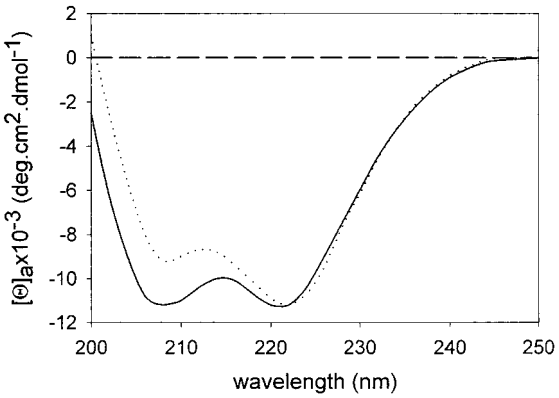

FIGURE 1: Far-UV CD spectrum of the chloride-induced A state (—). Experimental conditions: HCl, pH 2.2, and 25 °C. All the other anions investigated gave rise to far-UV spectra pratically identical, in shape and intensity, to that illustrated in the figure (the effect of the nitrate and iodide could not be monitored, due to the excessive absorption). The spectrum of the native protein (···), run in 0.1 M phosphate buffer and pH 7.0, is shown for comparison.

RESULTS

The salt effect on acid-unfolded cyt *c* has been investigated by choosing anions (as sodium salt) carrying the same charge but displaying a different ionic radius. This choice allows selective detection of anion size-dependent effects. Anions used are here listed as a function of increasing ionic radius: chloride (1.36 Å), bromide (1.95 Å), nitrate (1.96 Å), iodide (2.16 Å), perchlorate (2.45 Å), trichloroacetate (3.40 Å). As will be described below, we found that the chloride, nitrate, and bromide (i.e., the small anions) stabilize an A state with tertiary structure differing from that stabilized by the perchlorate, iodide and thrichloroacetate (i.e., large anions). Here we shall describe and compare the effect produced on the protein by chloride and perchlorate, taken as representative for the small- and large-size anions, respectively.

Structural Properties of the Salt-Induced Intermediates. Figure 1 shows the far-UV CD spectrum (200−250 nm, which probes the secondary structure) of acid-denatured cyt *c* in the presence of chloride, compared to that of the native protein. The anion stabilizes the A state, inducing in the denatured protein a nativelike α-helix structure (*12*). The perchlorate as well as the other anions investigated produced a similar effect (not shown), though the concentration needed to induce protein collapse into the compact state depended on the type of anion. The titration curves of Figure 2 clearly show the higher efficiency of larger anions in the stabilization of the A state.

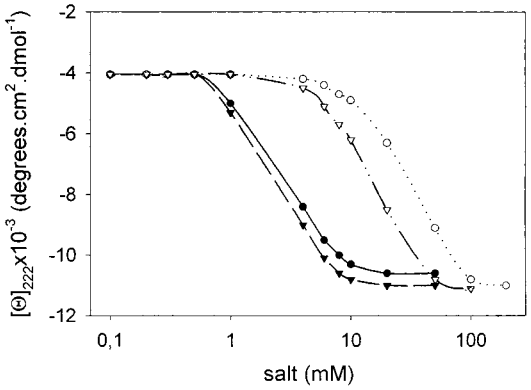

FIGURE 2: Salt-induced conformational transitions of denatured cyt *c* in HCl, pH 2.2, measured by the ellipticity at 222 nm at 25 °C. Anions investigated (all sodium salt) were: chloride (○); bromide (▽); perchlorate (●); trichloroacetate (▼).

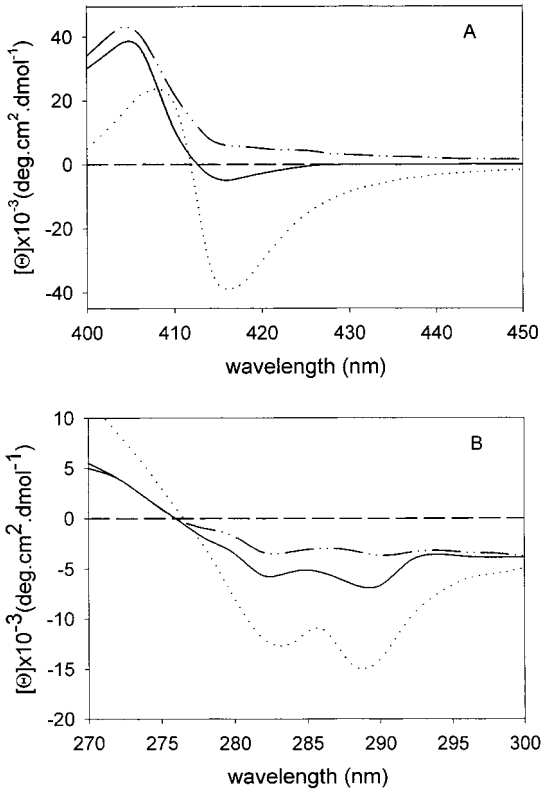

FIGURE 3: Soret (panel A) and near-UV (panel B) CD spectrum of the chloride (—)- and perchlorate-induced (— ·· —) A state of cyt *c*. Other experimental conditions as described to legend of Figure 1. The spectrum of the native protein (···) is shown for comparison.

Figure 3A shows the effect of the chloride and perchlorate on the Soret CD spectrum (400−450 nm, directly related to the structure of the heme pocket) of acid-denatured cyt *c*. Upon addition of salts, the native negative Cotton effect at 416 nm, ascribed to the Phe82− and Met80−heme interaction and diagnostic for the environment near the Met80−Fe(III) axial bond in the wild-type protein (*23*), is partly recovered in chloride, but not in perchlorate (see Figure 3). The lack of the 416 nm Cotton effect in perchlorate, reflecting an increased distance between the residues Phe82, Met80, and the heme group, reveals the lack of a direct interaction between the heme and the 70−85 residues polypeptide segment, which is thus expected to have enhanced mobility. As shown in Figure 3B, the near-UV

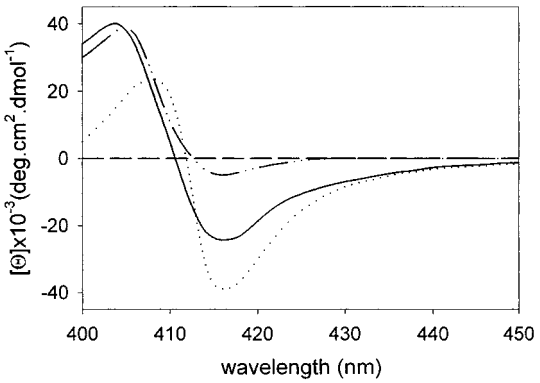

FIGURE 4: Soret CD spectrum of the chloride-induced A state of cyt *c*, recorded at 2 °C (—) and 25 °C (— ·· —). Other experimental conditions as described to legend of Figure 1. The spectrum of the native protein (···) is shown for comparative purposes.

dichroic spectrum of the native protein is characterized by two negative Cotton effects at 284 and 289 nm, attributed to the interaction between Trp59 and one heme propionate (*24*); such interaction is lost in the acid-denatured cyt *c*, as revealed by the absence of the two dichroic bands (spectrum not shown). As illustrated in the figure, in chloride, the two Cotton effects are partly recovered, their intensity being about one-third that of the native state, while in perchlorate the broad and weak bands of the dichroic spectrum (which almost overlaps that typical of the denatured protein) provide evidence for the absence of any significant Trp59−propionate group interaction. The smaller nitrate and bromide were found to act like the chloride, while the larger iodide and trichloroacetate like the perchlorate.

The 416 nm Cotton effect shown by the acid-unfolded cyt *c* in the presence of chloride is weaker than that of the native protein; to better understand the reason for such discrepancy, we followed the CD signal of the chloride-induced A state as a function of the temperature, in the 25−2 °C range. In chloride, the Soret CD is significantly affected by the temperature, as shown in Figure 4. At low temperature the intensity of the 416 nm Cotton effect increases and the spectrum becomes reminescent of that of the native protein. The observed temperature-dependent effect probed to be fully reversible. A similar temperature dependence was observed in the near-UV (at low temperature, the intensity of the 284 and 289 nm Cotton effects increases; spectrum not shown). For cyt *c*, the near-UV and Soret CD are diagnostic for the Trp59 and Phe82 (and Met80) state, respectively; this suggests that the flexibility of the 36−61 and 75−87 residue loops is influenced by temperature. As the temperature increases, the enhanced loops mobility causes a drop in the strength of the Trp59−heme propionate and Phe82−heme interactions. Conversely, no change was monitored in the far-UV region; this indicates that the hydrophobic core, composed by the main α-helix segments (*13*, *16*, *18*), is not influenced by temperature in the range investigated. In perchlorate, no temperature-induced CD change was detected in each of the regions investigated (not shown).

The structural properties of the anion-induced A state were also monitored by dynamic fluorescence measurements. Dynamic fluorescence technique is successfully employed for monitoring changes in the tertiary structure of proteins, by measuring the lifetime values of tryptophan residues. In the study of cyt *c*, the measurement of the fluorescence decay

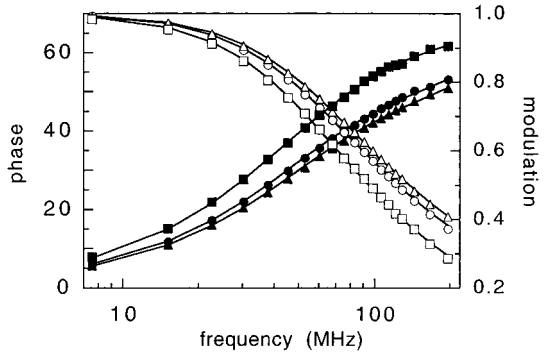

FIGURE 5: Dynamic fluorescence measurements for the native protein (squares), the chloride- (circles), and perchlorate-induced (triangles) A states. Phase (full symbols) and modulation (empty symbols) data are reported as a function of the modulation frequency of the excitation laser beam. Other experimental conditions as described to legend of Figure 1.

Table 1: Dynamic Fluorescence Parameters for the Chloride- and Perchlorate-Induced A State of Cyt *c*[a]

	exponential fit		exponential fit				
sample	χ^2	τ (ns)	χ^2	τ_1 (ns)	τ_2 (ns)	F_1	$\langle\tau\rangle$ (ns)
native	221	2.46	1.1	0.40	3.10	0.10	1.85
Cl^-	398	1.78	1.1	0.46	2.73	0.22	1.31
ClO_4^-	399	1.62	1.0	0.45	2.59	0.25	1.18

[a] Experimental conditions: HCl solution, pH 2.2; the temperature was 25 °C. Data relative to the native protein (0.1 M phosphate buffer, pH 7.0) are reported for comparative purposes. Abbreviations: χ^2, reduced χ^2 value; F_1, fluorescence fractional amplitude of the first exponential decay component ($F_2 = 1 - F_1$). $\Delta\tau_1 \cong 30$ ps; $\Delta\tau_2 \cong 50$ ps. $\Delta F_1 \cong 0.02$ $\langle\tau\rangle \cong$ average lifetime value

provides information on the single Trp59 environment. Figure 5 shows the phase-shift and demodulation data, graphed as a function of the modulation frequency, for the chloride- and the perchlorate-induced A states, compared to the native protein. The parameters used for fitting the experimental curves (using both a single- and a double-exponential decay) are reported in Table 1. Both data and fits indicate that the perchlorate-induced A state displays a different fluorescence decay from that of the native protein, diagnostic of distinct tertiary conformations. The chloride-induced state shows an intermediate behavior, which is indicative for a conformational state closer to that of the native protein, at level of the Trp59 surrounding. The evaluated average lifetime values, reported in Table 1, demonstrate that Trp59 experiences the strongest quenching effect in the perchlorate-induced state; this finding, which is in agreement with the steady-state fluorescence intensity (data not shown), likely reflects an enhanced accessibilty of the triptophan side chain to the solvent molecules, indicative for a high mobility of the 36−61 residues loop. In conclusion, both fluorescence and CD data support the view that chloride and perchlorate stabilize A states of cyt *c* having nativelike α-helix structures, but distinct tertiary conformations.

To get deeper insight, EPR measurements of the chloride- and perchlorate-induced A states were performed, as shown in Figure 6. The EPR spectrum of acid-denatured cyt *c*, shown in Figure 6a, shows no low-spin signal (characteristic of the native protein), but only an axial high-spin signal diagnostic for the rupture of the iron(III) coordination bonds. Addition of salts induces refolding of the protein as noted

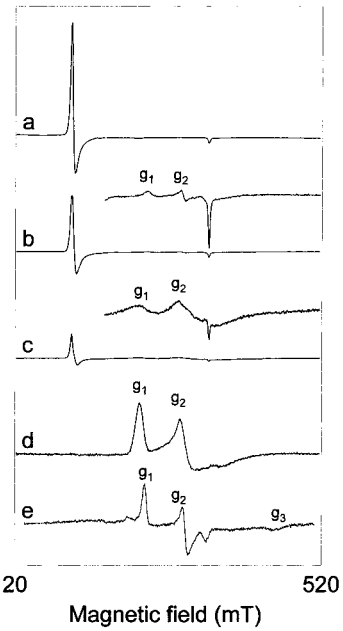

FIGURE 6: X-band EPR spectrum of acid-denatured cyt *c* (a), of the perchlorate (b)- and chloride-induced (c) A state. The spectrum of the native protein (d) and that of the Im-complex of carboxymethylated cyt *c* (e) are shown for comparative purposes. X-band EPR spectra were run at 5 K; protein concentration, 0.2 mM. Setting conditions were 9.42 Ghz microwave frequency; 20 mW microwave power; 0.10 mT modulation amplitude.

by the decrease of the high-spin component, associated to the appearance of a low-spin species which is characterized by *g* values strictly depending on the type of salt added. It must be noticed, however, that independently of the presence of the type of anions, there is always an equilibrium mixture of high and low-spin forms. In detail, addition of perchlorate (Figure 6b) gives rise to a low-spin state characterized by $g_1 = 2.87$ and $g_2 = 2.27$, while the g_3 is not measurable being its line too broad; a similar signal was observed for a nonhindered bis-4-methylimidazole complex (*25*), thus suggesting that the denatured protein collapses into a form with the heme iron coordinated to two histidine residues. This is confirmed by the EPR spectrum of the Im-complex of carboxymethylated cyt *c*, shown in Figure 6e. The spectrum, which surely belongs to a bis-histidine heme iron, is characterized by $g_1 = 2.96$, $g_2 = 2.26$, $g_3 = 1.48$, values close to those observed for the perchlorate-induced A state and indicating the same coordination; the slight differences observed, may be ascribed to different orientations of the imidazole ring (*29*). To our knowledge, this is the first time that the stabilization of a bis-imidazole equilibrium intermediate of cyt *c* is directly probed. The high−low-spin equilibrium here detected by EPR correlates well to the high- and low-spin intermediates detected by fast kinetics measurements during the cyt *c* folding (*26*−*28*). Addition of chloride gives rise to a low-spin species characterized by $g_1 = 3.07$ and $g_2 = 2.20$, as shown in Figure 6c. This signal is diagnostic for the Met80−Fe(III) axial coordination bond and is shown also by native cyt *c* reported in Figure 6d (*24*). However, the signal of the salt-induced state shows a line width larger than that of the native state, indicating a higher degree of structural heterogeneity (*30*). The EPR shows that the heme coordination depends on the type of anion present in solution, even though a compact state is always achieved.

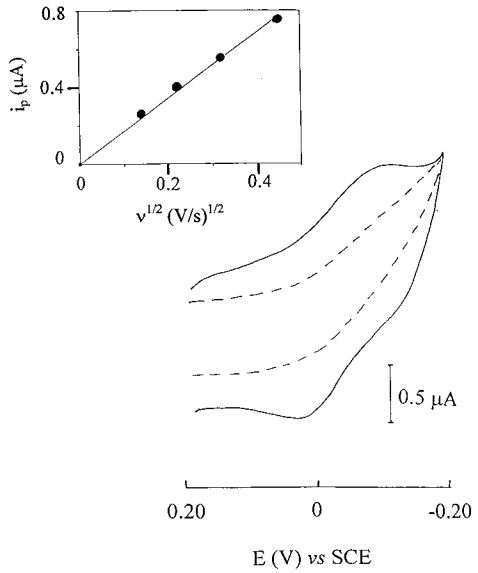

FIGURE 7: Dc cyclic voltammograms of the chloride (—)- and perchlorate-induced (- - -) A state of cyt *c*, run at a gold electrode chemically modified with 6-mercaptopurine. Protein concentration: 0.4 mM. Scan rate: 100 mV s^{-1}. Other experimental conditions as described to legend of Figure 1. Inset shows a plot of i_p vs (scan rate)$^{1/2}$.

The importance of the anion size in affecting the structural properties of the forming intermediate is observed also through the analysis of the high-spin component, which in chloride shows a line width larger (9.8 mT) than in perchlorate (7.5 mT), indicating the presence of a different microenvironment (*31*).

Redox Properties of the Salt-Induced Intermediates. The redox properties of the salt-induced A states were investigated by dc cyclic voltammetry. This technique provides important information on the heterogeneous electron-transfer kinetics between diffusing macromolecules and electrode surface and allows determination of the redox potential of the system investigated (*32*). Under the conditions investigated, no voltammetric signal is detected at a naked gold electrode; on the other hand, rapid electron transfer (eT) is observed in chloride at a gold electrode chemically modified with 6-MP. No electrochemical signal is observed in perchlorate. In chloride, the dc cyclic voltammograms of the protein exhibited a well-defined electrochemistry for scan rates ranging between 20 and 200 mV/s. Figure 7 shows the dc cyclic voltammogram run at 100 mV/s; the cathodic and anodic waves are similar in shape and magnitude, with a peak intensity ratio i_a/i_c close to unity. The peak separation, $\Delta E_p = 134 \pm 6$ mV, is larger than the theoretical value ($\Delta E_p = 57$ mV at 25 °C) for a fully reversible one-electron-transfer reaction (*33*). We found that ΔE_p increases at increasing scan rates, its value ranging between 107 ± 5 mV (at 20 mV/s) and 181 ± 10 mV (at 200 mV/s). As shown in the inset to Figure 7, i_p is proportional to the square root of the scan rate, indicating that the redox process is diffusion-controlled. The peak separation, larger than that shown by the native protein (*34*) and diagnostic for a slower eT rate, may reflect a perturbation in the heme pocket region likely in proximity of Phe82 and Met80, two side chains known to be involved in the eT process. The redox potential, $E_{1/2} = 233 + 5$ mV vs NHE, (determined from the espression $E_{pa} = E_{1/2} - \Delta E_p/2$) is close to that of the native protein ($E_{1/2} = 255$ mV vs NHE, at pH 7.0 and 25 °C), indicating that Met80 is coordinated to the heme iron. This is furtherly confirmed by the absorbance spectrum recorded in the 660−750 nm range, shown in Figure 8, where the 695 nm-band [attributed to the Met80-Fe(III) axial bond (*35*)] is clearly observable. On the other hand, the 22 mV drop in the redox potential value may reflect a weakened interaction between the iron-bound Met80 and Tyr67, indicative for an increased distance between the 60's helix and the heme group. Tyr67 is known to affect the heme redox potential of cyt *c* (*36*), since it modulates the Met80−heme iron axial bond strength [a 50 mV drop in the protein redox potential is observed, as this side chain is replaced (*37*)].

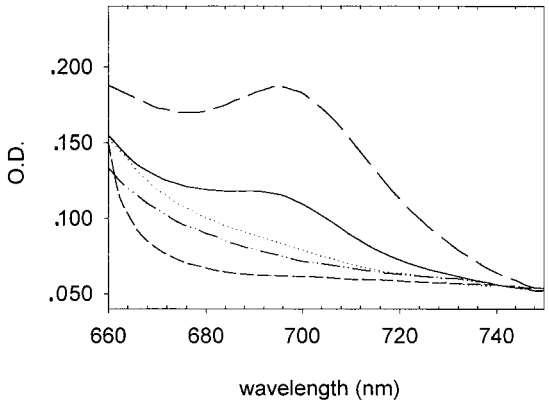

FIGURE 8: Absorbance spectra of chloride (—)- and perchlorate-induced (•••) A state of cyt *c* in the 660−750 nm range. Protein concentration: 0.25 mM. Other experimental conditions as described to legend of Figure 1. Spectra of acid-denatured (- - -) and native (— — —) cyt *c*, and of the Im-complex of the carboxymethylated derivative (— •• —), are shown for comparison.

No voltammetric signal was detected in perchlorate, under the same conditions, since the cyclic voltammogram recorded (shown in Figure 7) is almost superimposable to the baseline (not shown). This result is in disagreement with a previous report (*22*); however, the measurements, repeated several times, were always identical to those shown in Figure 7. We observed that the simple mixing of a HCl solution, pH 2.2, with a cyt *c* solution (final protein concentration 0.4 mM), without pH-adjustment, gives rise to a sharp cyclic voltammogram; however, in these conditions, the pH is over 3.0 and the displacement of Met80 from the sixth coordination position does not occur (as monitored by optical and CD spectroscopy). The procedure we used to achieve a 0.4 mM cyt *c* solution at pH 2.2, is described in detail in the Materials and Methods. The absence of a sharp voltammetric signal is well supported by the absorbance spectrum recorded in the 660−750 nm range (shown in Figure 8), which shows absence of peak at 695 nm.

In conclusion, the electrochemical data provide evidence that the chloride-induced A state shows nativelike redox properties, contrary to the perchlorate-induced A state. This underlines the relevant role played by the Met80 coordination to the iron, for the relatively high redox potential of cyt *c* (*38*−*40*).

Stability of the Salt-Induced Intermediates. Figure 9 shows the thermal denaturation profiles of the chloride- and perchlorate-induced A states of cyt *c*, as obtained from ellipticity values at 222 nm. The thermal transitions probed to be fully reversible. The shape of the unfolding profiles

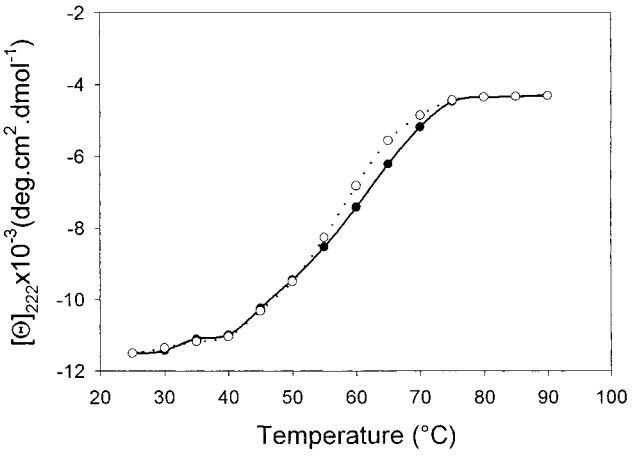

FIGURE 9: Unfolding profiles of the chloride (●)- and perchlorate-induced (○) A state of cyt *c*, as a function of increasing temperature. The experimental points refer to the ellipticity values at 222 nm. Other experimental conditions as described to legend of Figure 1.

excludes a simple two-state transition, since three distinct thermodynamic states (the A-state, a more extensively unfolded state, the denatured state) are detected (*41*, *42*). The unfolding profiles show that the chloride-induced A state is more stable than the perchlorate-induced one; however, the differences observed are very small, indicating that (i) the hydrophobic core (common to both the salt-stabilized forms) is the region that mainly contributes to the A state stability, and (ii) the Ω-loops are responsible for the spectroscopic differences observed.

DISCUSSION

Our data have shown that, under appropriate salt concentration, acid-denatured cyt *c* collapses into a compact state showing nativelike secondary structure but a tertiary conformation that strictly depends on the anion size. Small anions (ionic radius < 2.16 Å) induce formation of a compact, highly structured state, in which the native Met80−Fe(III) axial bond is recovered and the nativelike redox properties restored, although a bond between the iron and the other methionine present cannot be excluded. On the other hand, in the state stabilized by large anions (ionic radius > 2.16 Å), a histidine (His26 or His33) is ligated to the heme-iron at the sixth coordination position, the Trp59 side chain is more exposed to the solvent (while the H-bond with the heme propionate is severely weakened), and the macromolecule misses the functional properties typical of the native protein.

Goto and collaborators demonstrated that formation of the salt-induced A state of acid-denatured cyt *c* is achieved through an anion-binding mechanism and that the anion charge is the main determinant of salt effectiveness (*12*). In the present paper, we show that the fine 3D conformation of the A state strictly depends on the anion size, at least for single-charged anions. This scenario (i) suggests the presence in the macromolecule of binding sites discriminating anions as a function of their size, and (ii) shows a high sensitivity of the loops toward external agents, indicating that slight differences in the medium composition may push the protein toward different intermediate conformations, during folding. As matter of fact, various external factors, such as glycerol and sugars, were reported to induce the molten globule state of cyt *c* (*43*−*45*). On the other hand, the anion size does not affect the stability of the two anion-induced intermediates significantly. This indicates that the hydrophobic core [formed by the main α-helix segments (*13*, *16*, *18*)] is the region providing the strongest contribute to the A state stability, while the contribution of the highly flexible loop regions, responsible for the different spectroscopic and redox properties detected, appears negligible.

Englander and co-workers have proposed a sequential model (*19*) to describe the folding mechanism of cyt *c*. Under equilibrium condition, cyt *c* unfolds through a well-defined, fully reversible mechanism involving a small number of intermediate forms. Three are the partially unfolded forms detected, which represent the sequential intermediates in the unfolding-refolding process. According to the model, the unfolded protein is expected to refold by a pathway consisting of the same number of intermediate forms, stabilized by the step-by-step folding of cooperative units (Ω-loops or mutually stabilizing helices and loops), one unit at a time. As cooperative units, the model indicates five main segments (composed of about 15 residues) characterized by distinct unfolding energies. The loop formed by the 70−85 residues is the one with the lowest unfolding energy and, thus, the first segment to unfold under denaturing conditions (rupture of the native Met80−Fe(III) axial bond occurs at this stage); this means that its formation marks the final step during the protein folding. According to the model, the next segment to unfold is the 36−61 residues loop (i.e., that containing Trp59), then followed by the three segments constituting the more stable hydrophobic core, i.e., the helical segments.

In the present paper, we have shown that binding of small anions to the acid-unfolded protein induces formation of a highly structured, low-spin state in which the native Met80−Fe(III) bond, essential for the stabilization of the native, biologically active conformation, is recovered. This implies refolding of the 70−85 residues loop, according to the sequential model. Thus, small anions stabilize a state structurally close to the native and with nativelike redox properties. On the other hand, the Met80−Fe(III) bond is weakened. We ascribe this to the conditions employed; at neutral pH, the Met80−Fe(III) bond is strengthened, due to a number of hydrogen bonds between loops which decrease the loops mobility and stabilize the rigid, native protein conformation. At pH 2.2, this condition cannot be satisfied, due to the high proton concentration which leaves the protein with a high positive charge; as a result, the dynamic properties of the free loops are considerably enhanced. Thus, the axial bond might be weakened by the high degree of flexibility of the 70−85 residues loop. A similar conclusion may be reached to explain the reduced Trp59−heme propionate interaction observed (in this case, the loop involved is the 36−61 residues loop); support comes from a prior work reporting that Trp59 loses its tertiary hydrogen bond and is rotationally disordered in the A state, though remaining buried in a hydrophobic environment (*18*).

For the six-coordinate, low-spin state stabilized by large anions, a bis-histidine coordination is observed. Provided that His18 is one axial ligand of the heme-iron, the sixth coordination position must be occupied by one of the two other histidines present in the polypeptide chain, His26 or His33. This implies a different structure of the heme pocket, due to the lack of a direct interaction between the heme group

and the 70−85 residue loop which are connected, in the native protein, through the Met80 coordination to the iron. These structural changes affect the spectroscopy and the redox behavior of the intermediate, and point out the important role played by Met80 for a correct protein function. According to the sequential model, the intermediate appears less structured than that stabilized by small anions, since it misses the Met80−iron axial bond (and, thus, the interaction between the 70−85 residue loop and the heme), and the Trp59−heme propionate H-bond (which means lack of interaction between the 36−61 residues loop and the heme group), diagnostic for a more fluctuating tertiary structure. It is of interest the observation that a misfolded bis-histidine intermediate was recently detected by fast-kinetics studies on folding of cyt *c* (*26*, *27*).

In summary, anions fold acid-denatured cyt *c* into a compact state (the A state) possessing nativelike secondary structure. On the other hand, the anion size affects the protein tertiary conformation; small anions stabilize an A state with the native Met80−Fe(III) axial bond recovered and the native redox properties restored, whereas large anions stabilize bis-histidine coordinated form, in which the two heme ligands are the native His18 and a misligated His26 or His33. Despite this, the two forms show close thermal stability, suggesting that the hydrophobic core (common to both the anion-induced forms) is the region providing the most relevant contribute to protein stability.

REFERENCES

1. Creighton, T. E. (1990) *Biochem. J. 270*, 1−15.
2. Kim, P. S., and Baldwin, R. L. (1990) *Annu. Rev. Biochem. 59*, 631−660.
3. Dill, K. A., and Chan, H. S. (1997) *Nat. Struct. Biol. 4*, 10−19.
4. Dobson, C. M. (1992) *Curr. Opin. Struct. Biol. 2*, 6−12.
5. Kuwajima, K. (1989) *Proteins: Struct., Funct., Genet. 6*, 87−103.
6. Ptitsyn, O. B. (1992) in *Protein folding* (Creighton, T. E., Ed.), pp 243−300, Freeman and Company, New York.
7. Baldwin, R. L. (1991) *Chemtracts-Biochem. Mol. Biol. 2*, 379−389.
8. Christensen, H., and Pain, R. H. (1991) *Eur. Biophys. J. 19*, 221−229.
9. Barrick, D., and Baldwin, R. L. (1993) *Protein Sci. 2*, 869−876.
10. Kuwajima, K. (1996) *FASEB J. 10*, 102−109.
11. Goto, Y., Calciano, L. J., and Fink, A. L. (1990) *Proc. Natl. Acad. Sci. U.S.A. 87*, 573−577.
12. Goto, Y., Takahashi, N., and Fink, A. L. (1990) *Biochemistry 29*, 3480−3488.
13. Jeng, M. F., Englander, S. W., Elove, G. A., Wand, A. J., and Roder, H. (1990) *Biochemistry 29*, 10433−10437.
14. Goto, Y., and Nishikiori, S. (1991) *J. Mol. Biol. 222*, 679−686.
15. Kataoka, M., Hagihara, Y., Mihara, K., and Goto, Y. (1993) *J. Mol. Biol. 229*, 591−596.
16. Marmorino, J. L., and Pielak, G. J. (1995) *Biochemistry 34*, 3140−3143.
17. Marmorino, J. L., Lehti, M., and Pielak, G. J. (1998) *J. Mol. Biol. 275*, 379−388.
18. Jordan, T., Eads, J. C., and Spiro, T. G. (1995) *Protein Sci. 4*, 716−728.
19. Bai, Y., Sosnick, T. R., Mayne, L., and Englander, S. W. (1995) *Science 269*, 192−197.
20. Gratton, E., Jameson, D. M., and Hill, R. (1984) *Annu. Rev. Biophys. Bioeng. 13*, 105−124.
21. Beechem, J. M., and Gratton, E. (1988) *Proc. SPIE-Int. Soc. Opt. Eng. 909*, 70−81.
22. Pineda, T., Sevilla, J. M., Roman, A. J., and Blazquez, M. (1997) *Biochim. Biophys. Acta 1343*, 227−234.
23. Pielak, G. J., Oikawa, K., Mauk, A. G., Smith, M., and Kay, C. M. (1986) *J. Am. Chem. Soc. 108*, 2724−2727.
24. Moore, G. R., and Pettigrew, G. W. (1990) *Cyts c. Evolutionary, Structural and Physiological Aspects*, Springer-Verlag, Berlin.
25. Salerno, J. C., and Leigh, J. S. (1984) *J. Am. Chem. Soc. 106*, 2156−2161.
26. Takahashi, S., Yehm, S.-R., Das, T. K., Chan, C.-K., Gottfried, D. S., and Rousseau, D. L. (1997) *Nat. Struct. Biol. 4*, 44−50.
27. Yeh, S.-R., Takahashi S., Fan, B., and Rousseau, D. L. (1997) *Nat. Struct. Biol. 4*, 51−56.
28. Yeh, S.-R., and Rousseau, D. L. (1998) *Nat. Struct. Biol. 5*, 222−228.
29. Rifkind, J. M., Aburgo, O., Levy, A., and Heim, J. (1994) *Methods Enzymol. 231*, 449−480.
30. Bizzarri, A. R., and Cannistraro, S. (1992) *Appl. Magn. Res. 3*, 1033−1043.
31. Bizzarri, A. R., and Cannistraro, S. (1993) *Eur. Biophys. J. 22*, 259−267.
32. Bond, A. M. (1980) *Modern Polarographic Methods in Analytical Chemistry*, Marcel Dekker, Inc., New York.
33. Nicholson, R. S., and Shain, I. (1965) *Anal. Chem. 36*, 706−723.
34. Szucks, A., and Novak, M. (1995) *J. Electroanal. Chem. 383*, 75−84.
35. Stellwagen, E., and Cass, R. (1974) *Biochem. Biophys. Res. Commun. 60*, 371−375.
36. Brayer, G. D., and Murphy, M. P. (1996) in *Cyt c. A Multidisciplinary Approach* (Scott, R. A., and Mauk, A. G. Eds.) pp 103−166, University Science Book, Sausalito, CA.
37. Berghuis, A. M., Guillemette, J. G., Smith, M., and Brayer, G. D. (1994) *J. Mol. Biol. 235*, 1326−1341.
38. Raphael, A. L., and Gray, H. B. (1989) *Proteins: Struct., Funct., Genet. 6*, 338−340.
39. Raphael, A. L., and Gray, H. B. (1991) *J. Am. Chem. Soc. 113*, 1038−1040.
40. Ferri, T., Poscia, A., Ascoli, F., and Santucci, R. (1996) *Biochim. Biophys. Acta 1298*, 102−108.
41. Potekhin, S., and Pfeil, W. (1989) *Biophys. Chem. 34*, 55−62.
42. Kuroda, Y., Kidokoro, S., and Wada, A. (1992) *J. Mol. Biol. 223*, 1139−1153.
43. Davis-Searles, P. R., Morar, A. S., Saunders, A. J., Erie, D. A., and Pielak, G. J. (1998) *Biochemistry 37*, 17048−17053.
44. Santucci, R., Polizio, F., and Desideri, A. (1999) *Biochemie 81*, 745−751.
45. Ali, V., Prakash, K., Kulkarni, S., Ahmad, A., Madhusudan, K. P., and Bhakuni, V. (1999) *Biochemistry 38*, 13635−13642.

BI000516V